

Mobile Platform Pushbroom Sensor Motion Control, Image Corrections and Spectral Band Selection: Examples of Hyperspectral Imagery Using Low Flying Aircraft and Small Vessels in Coastal Littoral Areas

Charles R. Bostater¹, Gaelle Coppin², Florian Levaux²,
James Jones³, Heather Frystacky³

Environmental Optics Laboratory and Remote Sensing Center, College of Engineering
Florida Institute of Technology, 150 West University Blvd., Melbourne, Florida, USA 32901

ABSTRACT

Collection of pushbroom sensor imagery from a mobile platform requires correction of the platform motions using inertial measurement units (IMU's) as well as DGPS in order to create useable imagery for environmental monitoring and surveillance of shorelines in freshwater, littoral or harbour areas. This paper will present a suite of imaging systems used during collection of hyperspectral imagery during recent northern Gulf of Mexico airborne missions to detect weathered oil in coastal littoral zones. Underlying concepts of pushbroom imagery, the needed corrections for directional changes using DGPS and corrections for platform yaw, pitch, and roll using IMU data is described as well as the development and application of optimal band and spectral region selection for developing remote sensing algorithms. Pushbroom sensor and frame camera data collected in response to the recent Gulf of Mexico oil spill disaster will be presented as the scenario documenting the environmental monitoring and surveillance techniques using mobile sensing platforms. Data was acquired during the months of February, March, April and May of 2011. The low altitude airborne systems include a cooled hyperspectral imaging system with 1024 spectral channels and 1375 spatial pixels flown at 3,000 to 4,000 feet. The hyperspectral imaging system is collocated with a full resolution high definition video recorder for simultaneous HD video imagery, a 12.3 megapixel digital images for multispectral "sharpening" the hyperspectral imagery, a large frame 9 inch film mapping camera that yields scanned aerial imagery with approximately 2200 by 2200 pixel multispectral imagery (255 megapixel RGB images. Two high spectral (252 channels) and radiometric sensitivity solid state spectrographs are used for collecting upwelling radiance (sub-meter pixels) and a downwelling irradiance using a fiber optic irradiance sensor. These sensors are utilized for cross calibration and independent acquisition of ground or water reflectance signatures and for calculation of the bi-directional reflectance distribution function (BRDF). Methods are demonstrated for selecting optimal spectral regions and bands for discrimination, detection and characterization of weathered oil in the Northern Gulf of Mexico in response to the Deepwater Horizon oil spill disaster. The imagery presented and described allow for modern research in the use of sun and sky glint regions in imagery to identify water surface wave field characteristics as well as oil slicks. The systems described provide unique data sets of for modern airborne or satellite remote sensing algorithm development and future testing of radiative transfer models useful in studying the environment at small spatial scales.

Keywords: image analysis, submerged targets, calibration, hydrologic optics, airborne sensors, airborne imagery, hyperspectral sensing, multispectral imagery, radiative transfer, subsurface feature extraction, cameras.

1. INTRODUCTION

1.1 Background

Large field of view sensors as well as flight line tracks of hyperspectral reflectance signatures are useful for helping to help solve many land and water environmental management problems and issues. High spectral and spatial resolution sensing systems are useful for environmental monitoring and surveillance applications of land and water features, such as species discrimination, bottom top identification, and vegetative stress or vegetation dysfunction assessments¹. In

¹Corresponding Author: bostater@fit.edu; phone 321-258-9134; fax 321-600-9412. ² Royal Military Academy, Brussels, Belgium - Atlantis Stars dual degree EU-US students, ³ Atlantis STARS students - Florida Institute of Technology.

order to help provide information for environmental quality or environmental security issues, it is safe to say that there will never be one set of sensing systems to address all problems. Thus an optimal set of sensors and platforms need to be considered and then selected. The purpose of this paper is to describe a suite of sensing systems that have been integrated and used on mobile platforms useful for land and water related assessments. Descriptions of instruments calibrations are also presented. Recently collected selected imagery and data are presented from flights and a vessel that operating in the littoral zone. Platform integration, modifications and sensor mounting was achieved using designated engineering representative (DER) analyses, and related FAA field approvals in order to satisfy safety needs and requirements. Specifically, methods for correcting HSI imagery for mobile platform motions and algorithms useful for selection optimal bands and spectral regions using airborne, fixed platforms or small vessels are presented that address the use of sensing platforms in assessing the Deepwater Horizon Gulf of Mexico disaster.

2. METHODS

2.1 Imaging Systems, Sensor Systems and Calibration

Photogrammetric imagery reported in this paper were obtained using traditional 9 inch mapping cameras utilizing 12 inch focal length cones, and using Kodak color negative film, AGFA panchromatic or color films, and Kodak color infrared film. When using AGFA panchromatic negative film (with extended UV and IR spectral response), one can also use a blocking filters, such as a Kodak Wratten # 70, that result in imaging a narrow band of light in the vegetative red edge. This allows the collection of the red edge feature in land vegetation or shallow water submerged vegetation. Airborne imagery shown in this paper was collected at 1,225 m between 10 AM local time or 4 PM local, with a 1/225 second shutter speed and aperture adjusted for optimal contrast and exposure. The large format (9 in²) negatives scanned at 2400 dpi using a scanner and a special glass plate obtained from Scanatron, Netherlands allows for minimization of “newton rings” in the resulting ~255 megapixel multispectral imagery shown below (left image). Experience has shown that this method works well with AGFA X400PE1 film. The aerial negative scanning process is calibrated using a scanned target with known sub-millimeter scales 0.005 mm to 5 um resolution using a 2400 dpi scanner. The film scanning process results in three band multispectral images with spectral response curves published by the film manufacturer (Agfa or Kodak). *In-situ* targets are used for calibration of the imagery using a combination of white, black or gray scale targets as shown below in an airborne digital image (right).

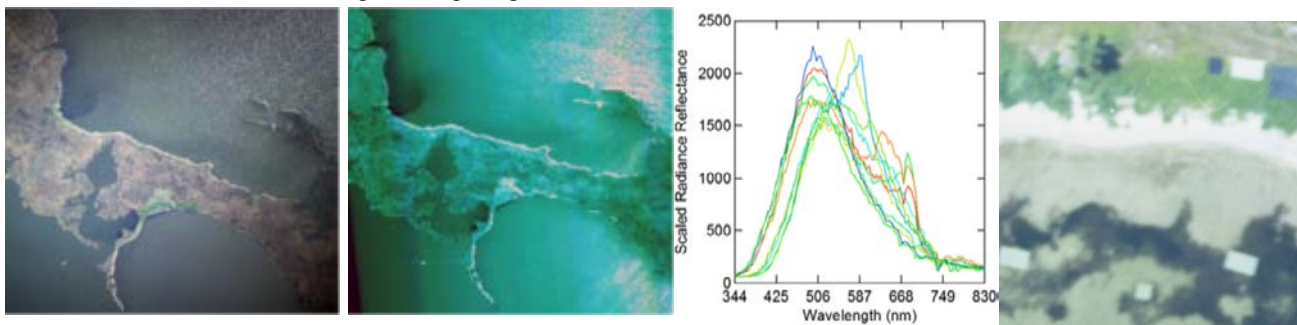


Figure 1. Example image (left) of a digitally scanned AGFA color negative film (X400PE1) from an airborne flight March 21, 2011 in Barataria Bay, Louisiana. The middle image is a simultaneously collected hyperspectral image showing 3 bands at 540, 532, 524 nm and both types of imagery demonstrates the ability to detect weathered oil released to the water column from oil spill remediation activities. The graph shows selected spectra from imagery in suspected weathered oil impact areas. Ground and *in-situ* water (submerged) targets (right) are used for image calibration, scale and pixel size verification from airborne flights

Airborne targets used for calibrating traditional film and digital sensor data for spatial and spectral characteristics using *in-situ* floating targets in the water as shown below. Targets are placed along the shoreline as shown above in an actual airborne scanned aerial image (above right) and as shown in Figure 2 below. Airborne “spectral color” targets have also been used as shown below and placed in the airborne scene before a flight. These types of land and water targets are used for image enhancement techniques, for use as GPS georeferencing ground control points, and georeferencing accuracy assessments. They are necessary in order to assess shoreline erosion estimation resulting from oil spill impacts.



Figure 2. *In-situ* water targets are used after precise GPS location is obtained (left) during deployment for image enhancement and georeferencing accuracy assessments. Black, white, gray and line targets (middle) are used for image and contrast adjustments of scanned aerial imagery and color targets (right) are used for spectral calibration purposes. Targets are required for accurate geospatial analysis such as coastal shoreline erosion and impact assessments due to weathered oil in marsh habitats.

Scanned film negatives result in approximately 255 megapixel images with approximately 22000 x 22000 pixels. A Nikon D2Xs 12.3 megapixel camera with a VR-NIKKOR 80-400mm lens with auto focus control and operated with an intervalometer is also used. The Nikon camera imagery is sequentially taken with the large frame camera(s) and synchronized with WAAS GPS with 5 HZ update encoded into the raw NEF image formats. Two full HD JVC 1920 x 1080p video cameras operating with a 30 HZ frame rate with GPS encoding (1 HZ) is also used for land and water surface imaging. One is located forward and another is collocated with the HSI imaging system. One is used for flight guidance and the other one is mounted next to the hyperspectral imaging system described below for platform motion corrections assessments.

The integrated hyperspectral imager (HSI) is a newly developed pushbroom sensor system with 1376 spatial pixels and a maximum of 1024 spectral channels. The HSI camera consists of a Cooke Corporation (PCO) Sensicam QE double shutter camera that is cooled to -12° C with stabilized Peltier 2 stage forced air cooler. The system allows for temperature stabilized 1024 to \sim 130 spectral channels with 12 bit digital resolution with extremely low dark current. The camera system can also be operated using software controlled CCD channel binning using the customized software developed in our lab. Scan lines are typically collected at approximately 25-80 HZ. A Motionnode IMU is strapped to the "gimbal mounted" HSI camera for collecting 3 axis motions (yaw, pitch and roll) data at 100 HZ. A Garmin 496 WAAS enabled GPS with 5 HZ position updates is integrated for scan line specific time, position, speed, direction and altitude data. All sensor data is time stamped using the system clock of a Fujitsu ST5112 tablet computer. A PCO camera fiber optical cable connects the camera to the computer via an external PCI image acquisition card that is interfaced to the pen tablet computer via a MAGMA PCMCIA card and cable to an external MAGMA external PCI bus box. A sophisticated software "pen tablet" program was written to control the HSI sensing system and acquire all sensor data streams. The software utilizes multithreading programming techniques to allow separate streams for controlling the HSI camera and SPECIM interchangeable spectrograph cores, IMU, and GPS. The spectrograph core based system utilizes interchangeable c-mount lenses produced for UV-VIS-NIR imaging applications produced by Schneider Optics. Separate data streams are stored on a hard disk with time stamps for each scan line in binary format. The software allows for real time image display and acquisition, selection of integration time and scan line delay time, sensor binning, as well as display of digital counts, spectral reflectance or radiance signatures. These displays allow for selection of optimal integration time in order to insure the full dynamic range of the sensor is utilized without saturation. The scan lines are stored in a ENVI readable image file format for post geometric processing using a Kalman filter/smoothing algorithm. Radiance is calculated using sensor calibration data for each spectral channel from sensor digital counts. Reflectance signatures are viewed in real time and as a real time image utilizing each scan line as a function of the aircraft flight path using calibration target grey panel data. The real time spectral signatures and imagery are essential for optimal control of the HSI camera integration time, and scan line delay time or sequencing. The integration time is set to optimize the digital and/or radiometric sensitivity of the camera for either: (a) water, (b) land surface or (c) combined land & water image acquisition. Reflectance measurements are calculated utilizing calibration grey panels before the flight, after the flight, or during the flight using an SE590 solid state spectrograph connected to a fiber optic cable and cosine corrected downwelling sensor. Post processing of the HSI system data stream involves converting the primary binary file types to

ASCII file types for use in Kalman filter based geometric correction, georectification and georegistration of the reflectance imagery.

2.2 Hyperspectral Imaging System Calibration

The hyperspectral imaging system was developed by integration of the Cooke - PCO Sensicam QE double shutter camera with either a ImSpector V10E (400 to 1,000 nm with ~ 2.8 nm spectral resolution) or V8E (380-800 nm with 2 nm spectral resolution) transmission spectrograph core. Either spectrograph allows use of the 2/3 inch CCD with full frame shutter operations of 25-80 HZ image acquisition using the PCI bus card and fiber optic connection to the camera and PCI camera controller.

The system uses a necessary blocking/cutoff filter for collection of correct spectral wavelengths and a variety of Schneider C mount lens (for various FOV's) with known transmission in the UV-VIS- NNIR spectral region and do not require refocusing across the spectrum. As indicated above, the software we developed allows for spatial and spectral binning. The Spectral response curve of the CCD is shown in Figure 3 below. The hyperspectral camera system is UV sensitive, and has excellent response for imaging clear natural waters due to its sensitivity in the blue region. The spectral response also shows high quantum efficiency near 532 nm and near the location of the reflectance “hinge point” commonly found as one travels from CASE I to CASE II and turbid, high chlorophyll water types.

The high quantum efficiency in the solar induced fluorescence region of ~698 nm is useful for water phytoplankton pigment detection as well as the “vegetative red edge” for shallow submerged sea grasses, “live corals”, and land vegetation. These factors make the camera a good selection for environmental monitoring and surveillance surveys. The UV sensitivity is useful for detecting surface films and *oil spill plumes* in water and littoral areas shown below.

We have found the UV sensitivity of the spectrograph and camera allows imaging just below ~350 nm. Use of a Baader UV transmission filter allows imaging in the UVB region or alternatively, a Wratten #18A, or Hoya U-340 UV transmission filter region for UV imaging. Custom made dual 20 inch calibration spheres acquired from Optronics Laboratories (Orlando, Florida) allow for spectral radiance calibrations. One is for low light calibration (useful for subsurface water imaging) as well as for standard outdoor illumination ranges.



Figure 3. Hyperspectral Imaging (HSI) System camera spectral response curve (left) and indicated important spectral regions for water surface film detection (oil plumes) in the UV, clear natural water (490 nm), water reflectance hinge point region (~532 nm), and the solar induced solar fluorescence for submerged sea grass, chlorophyll and “live corals”, and vegetation dysfunction in the “red edge” spectral region at 697 nm using the low light mode of the camera. Lower image are (right) the custom dual 20 inch calibration spheres for radiance and spectral wavelength calibrations of the HSI system.

Spectral line sources are used to generate a linear relation between the CCD channel and wavelength as shown in Figure 4 below. Linearity responses of the channels are excellent, even at low light levels in the UV channels (upper right).

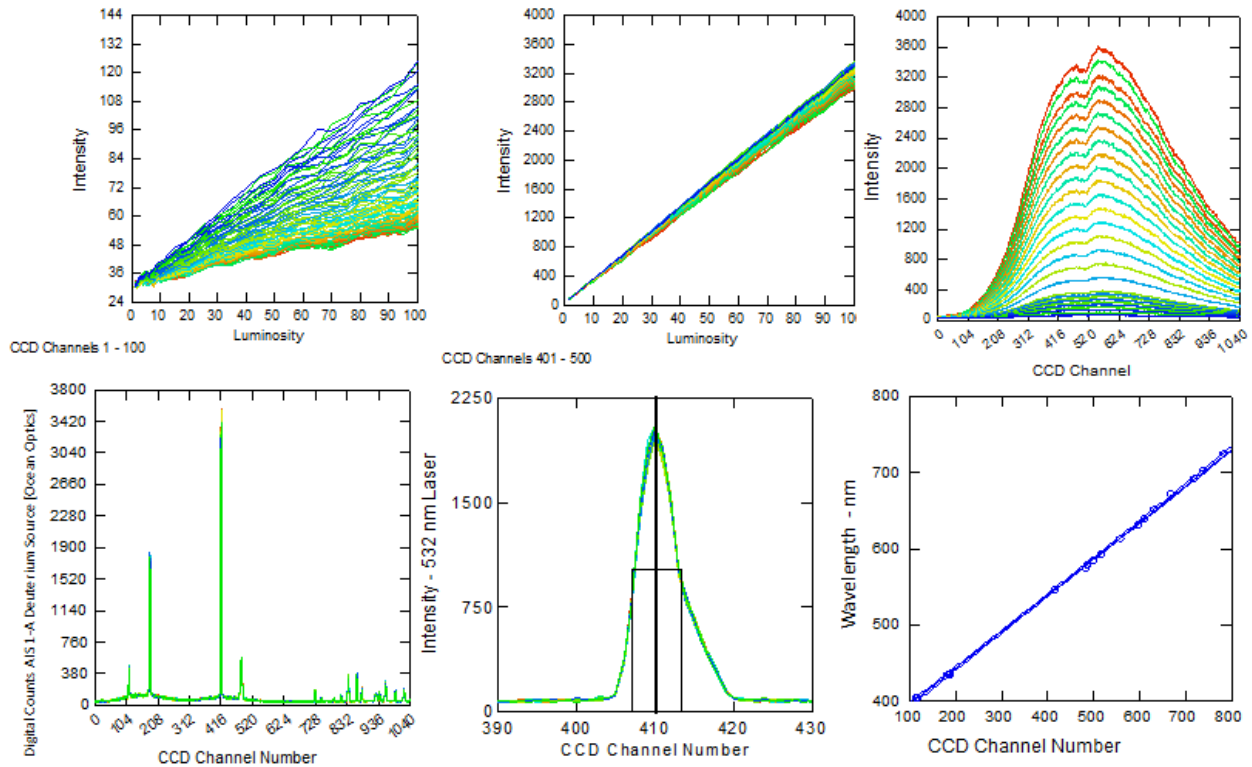


Figure 4. Calibrations of the hyperspectral pushbroom imaging system includes changing the calibration sphere light intensity (upper right) and obtaining the linear response for each spectral CCD channel (upper left low light UV channels) and upper middle (VIS channels). Spectral lines sources such as deuterium line sources and lasers (lower left, middle) allow CCD channel wavelength calibrations. The CCD channel and wavelength relation shown (lower right) shows excellent linearity for this HSI imaging system.

The HSI system utilizes C-mount UV-VIS-NIR transmission lenses. The pushbroom camera scan line field of view (FOV) needs to be calibrated using a laboratory based imaging track system - essentially translating optic bench system that was custom designed for HSI camera calibration purposes (see figure 5, below). In addition, the field of view is verified using flight line data after image rectification and georeferencing. The laboratory system is also used for alignment of the spectrograph core and the camera for spatial-wavelength-CCD channel adjustments and for lens focusing testing using laboratory targets for minimizing spectral smile and spatial keystone effects³.

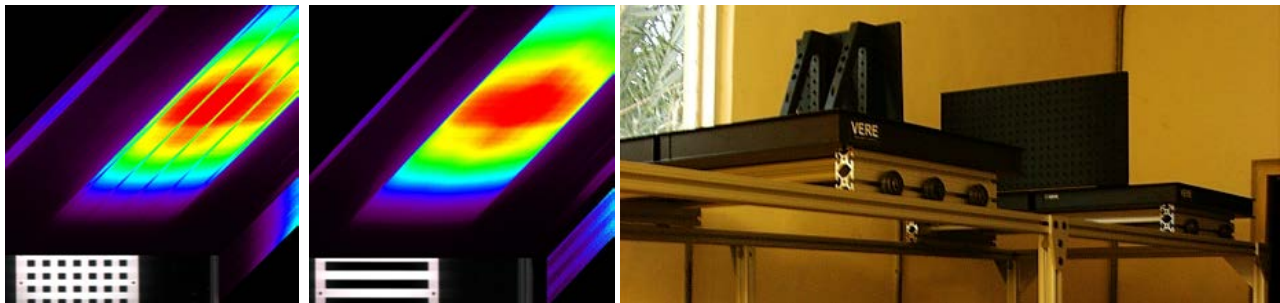


Figure 5. Example hyperspectral pushbroom “image cubes” collected of laboratory targets for calibration and adjustments of smile and keystone (left& middle) using a laboratory translating ~ 4 meter optical bench located ~ 2 meters above the targets spectrally calibrated targets.

Pushbroom calibration & testing in the laboratory and the field includes corrections to acquired hyperspectral imagery for yaw, pitch and roll of the mobile platform (ship, plane, or mobile vehicle). To assist in these corrections, a IMU was

utilized and mounted to the gimbale camera mount. Laboratory and field imagery was collected and IMU data collected between 60 and 100 HZ. Each scan line in an image is post processed with resampled IMU data, providing yaw, pitch and roll data. Outdoor image acquisitions are made using mobile platforms and include a WAAS 5 HZ GPS data collected for image hyperspectral image for rectification and georegistration along the sensor track in the lab or actual flight line⁴.

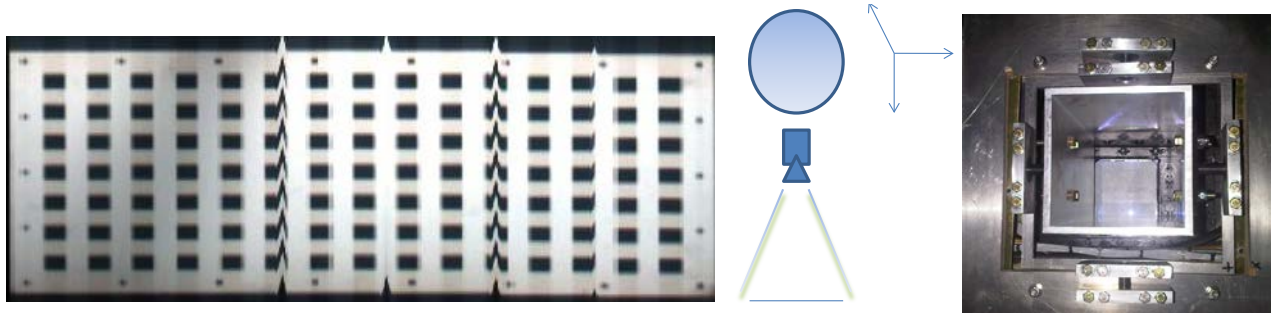


Figure 6. Laboratory HSI imagery (left) is collected using a translating optical bench with the HSI system mounted in the laboratory on a gimbale (right) camera mount and looking at the above target (left). An IMU mounted to the gimbale HSI camera collects yaw, pitch, roll and induced track curvature (measured with a GPS). Laboratory calibration and tests are conducted in the lab as well as outdoors (ambient imagery) in order to correct for laboratory controlled motion induced blurring during calibration and testing. Custom software is then used to post process and correct (rectify) the imagery before actual geo-registration and *panchromatic-multispectral-hyperspectral sharpening* of the hyperspectral imagery using specially designed software and algorithms. The above image (right) shows the influence of camera “roll” during an image collection sequence over a target in the laboratory.

2.3 Pushbroom Imagery Corrections for Platform Motions

Airborne pushbroom imagery collected aboard moving platforms (ground, air, sea, space) requires geometric corrections due to platform motions. These motions are due to changes in the linear direction of platform (flight direction changes), as well as sensor and platform motion due to yaw, pitch and roll motions. Unlike frame cameras that acquire a 2 dimensional image, pushbroom cameras acquire one scan line at a time. A sequence of scan lines acquired along the platform track allows the creation of a 2 dimensional image. The consequence of using this type of imaging system is that the scan lines collected produce spatial artifacts due to platform motion changes - resulting in scan line feature offsets. The following describes the roll induced problem to be corrected. Consider an airplane that is flying over a straight road indicated by the vertical line in the left image below. Now assume the airplane or mobile platform undergoes unwanted platform roll motion and thus the resulting straight feature in the acquired scene is curved, as suggested by the blue line in the left image. One knows that the road was straight so the image as shown in Figure 7(right) indicates a lateral scan line adjustment is required in order to straighten the feature (the blue line). This is accomplished by “shifting” the scan lines opposite to the platform roll motion and results in an image where the feature in the image is corrected. Thus, one needs to calculate the offset that corresponds to the shift the red points undergo.

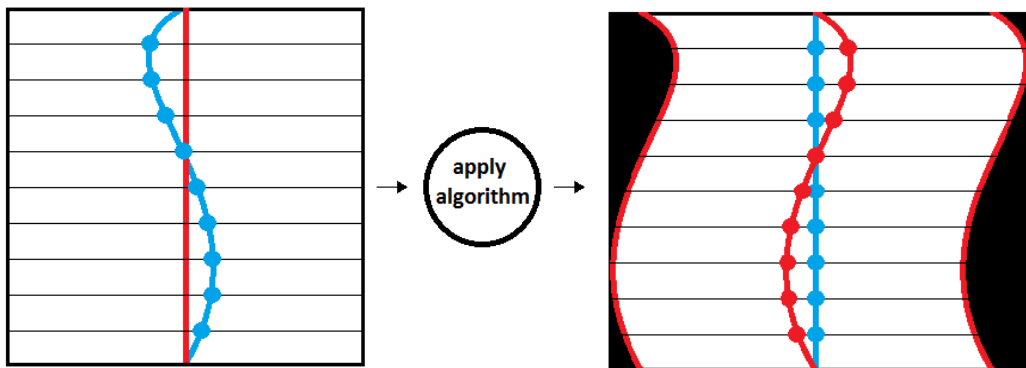


Figure 7. The left figure shows in blue a distorted road. The red line corresponds to the center of the scan line. The right image represents the corrected version of the left image. On this image the blue straight line is the road and the red curve is the actual position of the center pixels of the scan lines. In this example only the shift in the cross track direction is represented.

The offset mentioned previously can be corrected if sensing geometry and the HSI system orientations are known when the different scan lines were taken⁵. To obtain the platform and sensor orientation changes and position a 100 Hz update rate inertial measurement unit (IMU) was utilized and mounted to the gimbal mounted camera. In addition, differential WAAS 5 HZ GPS position, directional deviations, altitude from a specified datum, and platform speed are collected during the flights.

An adaptive Kalman filter is used for post processing or smoothing the induced platform motions using the combined sensor data from the GPS and IMU. The filtering technique thus allows one to obtain the relative position of each scan line and the corresponding spatial pixel shift that needs to be applied to correct the image. When a gimbal mounted HSI pushbroom camera is used, there are two main influences that cause the geometric distortions. These are the slowly varying directional changes of the platform and the roll induced motions. The first step in the algorithm is to use the GPS to calculate the position of the sensor (O_x, O_y, O_z) at every scan line. The second step accounts for the influence of the roll motion by using the IMU sensor data. The position of a pixel on the earth's surface can be estimated using⁵:

$$\begin{aligned}
 x &= O_x + \frac{s_x}{s_z} (h_{DEM} - O_z) \\
 y &= O_y + \frac{s_y}{s_z} (h_{DEM} - O_z) \\
 z &= h_{DEM}
 \end{aligned}
 \tag{2.1}$$

Where (s_x, s_y, s_z) are the components of the unit central scan line ray vector, (x, y, z) the position in meters compared to the origin (the position of the center of the scan line) and h_{DEM} the surface elevation given in meters.

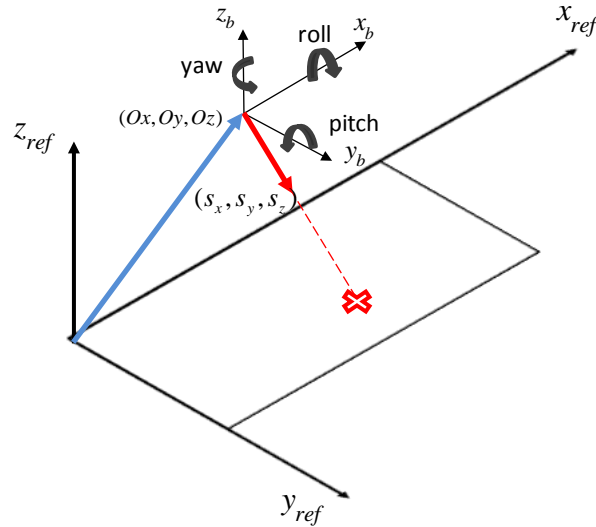


Figure 8. This figure shows the position of the sensor (O_x, O_y, O_z) and the unit scan line ray vector in the reference coordinate system as well as the body (sensor platform) coordinate system with the possible platform motions.

The reference coordinate system chosen in this paper is a local tangent plane with the x axis pointed in the initial along track direction, y axis is 90 degrees clockwise to the x axis and corresponds to the initial cross track direction. In the results that are presented in this paper, shifts have only been applied in the cross-track direction. The shifts in meters are scaled to shifts in pixels as a function of the altitude (given by the GPS), the field of view of the sensor (dependent upon the lens used) and the number of pixels in one scanline (1376 for the sensor used here).

The Kalman filter application consists of 2 steps. A temporal update step (also known as the “a priori” prediction step) and a measurement update step (also known as the “a posteriori” correction step). In the temporal step given by

equation⁶ 2.2, the estimated state vector and the estimation covariance of the next time step are predicted based on the current knowledge. The predictive procedure step is given by:

$$\begin{aligned}\hat{x}_k^- &= A_{k-1}\hat{x}_{k-1}^+ + B_{k-1}u_{k-1} \\ P_k^- &= A_{k-1}P_{k-1}^+A_{k-1}' + Q_{k-1}\end{aligned}\quad , \quad 2.2$$

and the measurement update step (given by equation 2.3 below) corrects the predicted estimated state vector (the position) based on additional sensor measurements to obtain the corrected estimate of the state vector or:

$$\begin{aligned}K_k &= P_k^-H_k'(H_kP_k^-H_k' + R_k)^{-1} \\ \hat{x}_k^+ &= \hat{x}_k^- + K_k(z_k - H_k\hat{x}_k^-) \\ P_k^+ &= (I - K_kH_k)P_k^-\end{aligned}\quad , \quad 2.3$$

where:

\hat{x}_k^- and \hat{x}_k^+ = respectively the predicted (-) and corrected (+) value of the estimated state vector,
 u = the control input vector.

P^- and P^+ are respectively the predicted and corrected value of the estimation covariance.

R = the covariance of the sensor noise also known as measurement uncertainty.

Q = the covariance of the dynamic disturbance noise.

H = the measurement sensitivity matrix also known as the observation matrix.

K = the Kalman gain.

The Kalman filter computes a weighted average of the predicted and the measured state vector by using the Kalman gain K . If we have an accurate sensor, the uncertainty on the measurement will be small so there will be more weight given to the measurement and thus the corrected estimate will be close to the measurement,. When one has a non-accurate sensor, the uncertainty on the measurement is large and more weight will be given to the predicted estimate. A Kalman smoother has been applied as well where the algorithm⁷ is shown in equation 1.4 below. This algorithm does not only use past observations, but incorporates future observations as well to estimate the state vector, or:

$$\begin{aligned}C_k &= P_k^+A_k^T(P_{k+1}^-)^{-1} \\ \hat{x}_k^s &= \hat{x}_k^+ + C_k(\hat{x}_{k+1}^s - A_k\hat{x}_k^+) \\ P_k^s &= P_k^+ + C_k(P_{k+1}^s - P_{k+1}^-)C_k^T\end{aligned}\quad 2.4$$

In the results that are presented in this paper, pixel shifts are only applied in the cross-track direction. Use of a gimbal sensor mount has allowed reduced HSI sensor motion corrections, however the need for improving image corrections in order to include pitch and yaw motions are currently being assessed. Results of the above are shown section 3 of this paper.

2.4 Feature Detection in Hyperspectral Images Using Optimal Multiple Wavelength Contrast Algorithms

Hyperspectral signatures and imagery offer unique benefits in detection of land and water features due to the information contained in reflectance signatures that directly show relative absorption and backscattering features of targets. The reflectance spectra that will be used in this paper were collected *in-situ* on May 31st 2011 using a SE590 high spectral resolution solid state spectrograph and the HSI imaging system described above. Bi-directional Reflectance Distribution Function (BRDF)⁸ signatures were collected of weathered oil, turbid water, grass and dead vegetation. The parameters describing the function in addition to the wavelength λ , (368-1115 nm) were the θ_i (solar zenith angle) = 71.5°, θ_0 (sensor zenith angle) = 55°, ϕ_i (solar azimuth angle) = 105° and the ϕ_0 (sensor azimuth angle) = 270°. The reflectance BRDF signature is calculated from the downwelling radiance using a calibrated Lambertian diffuse reflectance panel and the upwelling radiance at the above specified viewing geometry for each target (oil, water, grass, dead vegetation) a described in the figure below.

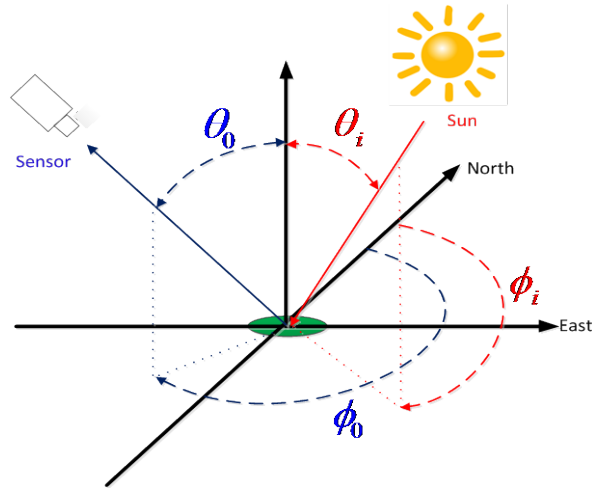


Figure 9. Illumination and viewing geometry defined for calculation of the BRDF signatures collected using the 252 channel SE590 high spectral and radiometric sensitivity solid state spectrograph and the hyperspectral imaging system, where θ_i is the incident solar zenith angle of the sun, θ_0 is the sensor zenith angle, ϕ_i is the solar azimuth angle from the north and ϕ_0 is the sensor azimuth angle as indicated above. In general, a goniometer measurement system is used to measure the BRDF in the field or laboratory environment as the sensor zenith and azimuth angles are changed during a collection period with a given solar zenith conditions.

The figures below show the results of measurements from 400 to 900 nm for a 1 mm thick surface weathered oil film, diesel fuel, turbid water (showing the solar induced fluorescence line height feature, dead vegetation, and field grass with the red edge feature common to vegetation and associated leaf surfaces). These BRDF signatures are used below to select optimal spectral channels and regions using optimally selected contrast ratio algorithms in order to discriminate oil from other land & water features in hyperspectral imagery collected as described in Section 2.5.

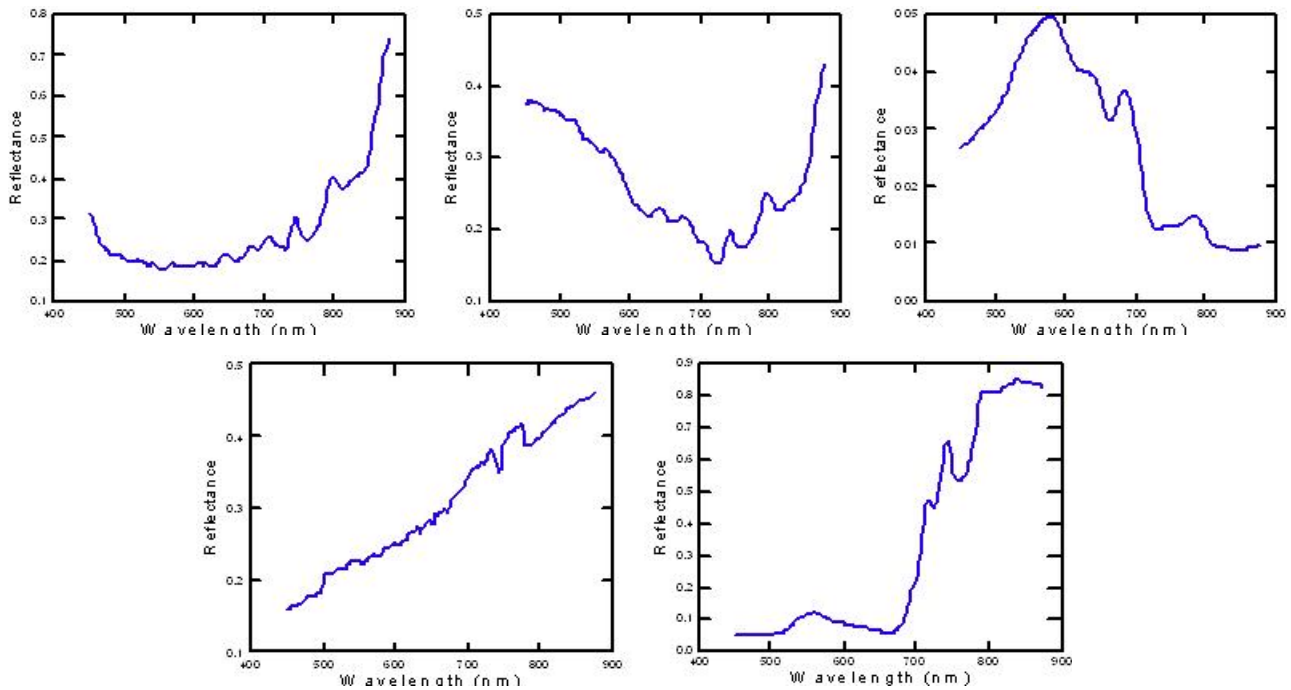


Figure 10. Averaged ($n=360$) BRDF reflectance spectrums collected using a SE590 solid state spectrograph May 31, 2010. From upper left to right: BRDF spectrum of weathered oil (1 mm thick film) on clear water, diesel film (1mm thick film) on clear water, turbid water, with high chlorophyll content as indicated by the solar induced fluorescence line height, dead vegetation (dead leaves) and field grass showing the red edge. Solar angles were determined from DGPS location, time of day, and sensor position angles and measured angle from magnetic north direction.

The above BRDF signatures were used to select optimal spectral regions in order to apply the results to hyperspectral imagery collected from a weathered oil impact shoreline in Barataria Bay, LA. The first method used was to perform feature detection using spectral contrast signature and HSI image contrast. The well know Weber's contrast^{9,10} definition is first used to determine the maximum (optimal) value of the contrast between a target t and a background b as a function of wavelength, or:

$$C_t(\lambda_k) = \frac{BRDF_t(\theta_0, \phi_0, \theta_i, \phi_i, \lambda_k) - BRDF_b(\theta_0, \phi_0, \theta_i, \phi_i, \lambda_k)}{BRDF_b(\theta_0, \phi_0, \theta_i, \phi_i, \lambda_k)} \quad 2.5$$

The resulting contrast calculated across the spectrum for each channel are shown below using the 1 mm thick oil film as the target and the backgrounds of turbid water, dead vegetation (dead foliage), and field grass.

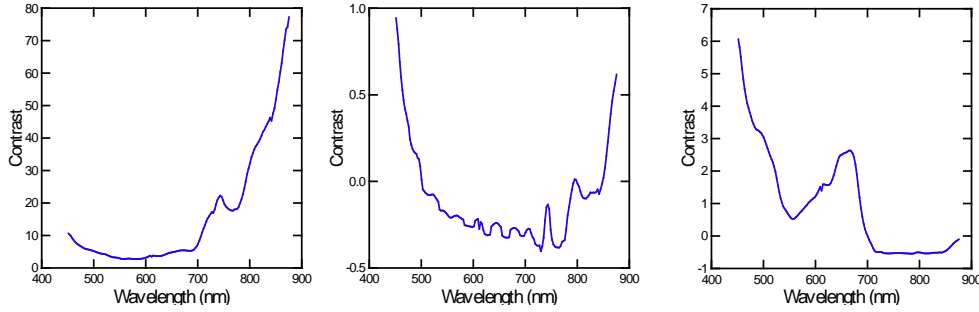


Figure 11. Resulting BRDF Weber contrast signatures between the oil as the target and different backgrounds. From left to right: turbid water, dead vegetation (dead foliage) and field grass.

The result of the optimization of the contrast as obtained from equation 2.5 will yield an optimal channel and/or spectral region as a function of wavelength where the contrast is maximized between a specified target and specified background or feature in a hyperspectral image collected from a fixed or moving platform.

A limitation with this common definition of the contrast is that one band is used out of all the possible combinations available in a hyperspectral image for the feature detection or extraction algorithm. This limitation can be overcome, by defining an advantageous “multiple-wavelength (or channel) contrast” as¹²:

$$\begin{aligned} C_t(\lambda_{k,m}) &= \frac{BRDF_t(\theta_0, \phi_0, \theta_i, \phi_i, \lambda_k) - BRDF_b(\theta_0, \phi_0, \theta_i, \phi_i, \lambda_{k\pm m})}{BRDF_b(\theta_0, \phi_0, \theta_i, \phi_i, \lambda_{k\pm m})} \\ &= \frac{BRDF_t(\theta_0, \phi_0, \theta_i, \phi_i, \lambda_k)}{BRDF_b(\theta_0, \phi_0, \theta_i, \phi_i, \lambda_{k\pm m})} - 1 \end{aligned} \quad 26$$

The result of the optimization of this “multiple-wavelength contrast algorithm” is given by the optimal selection of a band ratio (located in a spectral region) minus one. Furthermore, a new definition of the inflection contrast spectrum¹¹ (a numerical approximation of the second derivative) can be defined. The contrast inflection spectrum described in previous papers was given by:

$$I_t(\lambda_{k,m,n}) = \frac{BRDF_t(\theta_0, \phi_0, \theta_i, \phi_i, \lambda_k)^2}{BRDF_t(\theta_0, \phi_0, \theta_i, \phi_i, \lambda_{k+m}) BRDF_t(\theta_0, \phi_0, \theta_i, \phi_i, \lambda_{k-n})} \quad 2.7$$

where m and n are respectively defined as a dilating wavelet filter forward and backward operators described by Bostater, 2006. This inflection is used to estimate the second derivative of reflectance spectra. The underlying goal of computing an approximation of the second derivative is to utilize the nonlinear derivative based, dilating wavelet filter to enhance the variations in the reflectance spectra signals, as well as in the contrast spectrum signals. These variations directly represent the target and background absorption (hence: concave up) and backscattering (hence: concave down) features within a hyperspectral reflectance image or scene and form the scientific basis of the discrimination based

noncontact optimal sensing algorithms. A practical limitation encountered using this definition above, is that a concave-down (or backscattering) feature value of the inflection as defined in 2.7 is greater than one and a concave up (or absorption) feature, in the inflection or derivative based wavelet filter defined in 1.7 will be between 0 and 1. There is thus a difference in scale between a concave-up and a concave-down behavior. Consider the following example:

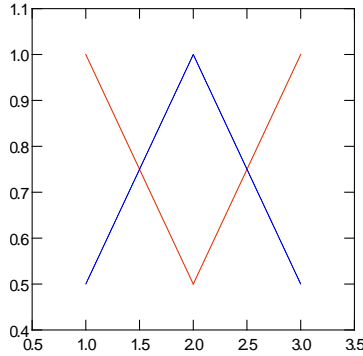


Figure12. Example concave-down (backscattering) feature (blue line) and a concave-up (absorption) feature (red line) of the same amplitude (Y axis) as a function of an spectral wavelength on the x axis.

In the case of the concave-down, the result of the inflection is:

$$I = \frac{1^2}{0.5 * 0.5} = 4$$

While in the case of the concave-up (same concavity), the result will be:

$$I = \frac{0.5^2}{1 * 1} = 0.25$$

To order to give equal weight to absorption and backscatter features in the band selection process, a modified spectrum for $I^*(\lambda)$ is define as:

$$I^* = \begin{cases} I & \text{for } I > 1 \\ -\frac{1}{I} & \text{for } 0 < I < 1 \end{cases} \quad 2.8$$

Using this definition, both concavities will be on the same scale and a concave-down feature (hence: backscattering) will give a positive value (>1) while a concave-up feature (hence: absorption) will give a negative value (<-1) and be treated the same numerically. For example, in the above example, the result for the new definition of the inflection or 2nd derivative estimator will be 4 and -4.

A second issue is to determine what values to assign to the upward and backward operators in the dilation filter. One could pick the optimal value for the inflection using all possible combinations of m and n. The problem with that method is that when m and n are too big, the difference between the channels for which the inflection is calculated and the one to which it is compared can be influenced by the signal to noise ratio being at the low and high wavelengths in a typical camera/spectrograph system. Thus the resulting optimal regions selected in can be scientifically or physically difficult to explain. So a limit to is placed on the maximum value of m, n operators from a practical point of view. The minimal value of m, n is 1. Thus, one can select the optimal range of the m and n wavelet filter operators (either a maximum (backscattering) or a minimum (absorption) for all combinations of m and n between 1 and the maximal value (in this paper this maximal value used was selected as 7). The resulting derivative estimator spectra (inflection spectra) using equation 2.8 is calculated and shown below, using the previously shown BRDF spectra shown in Figure10 above.

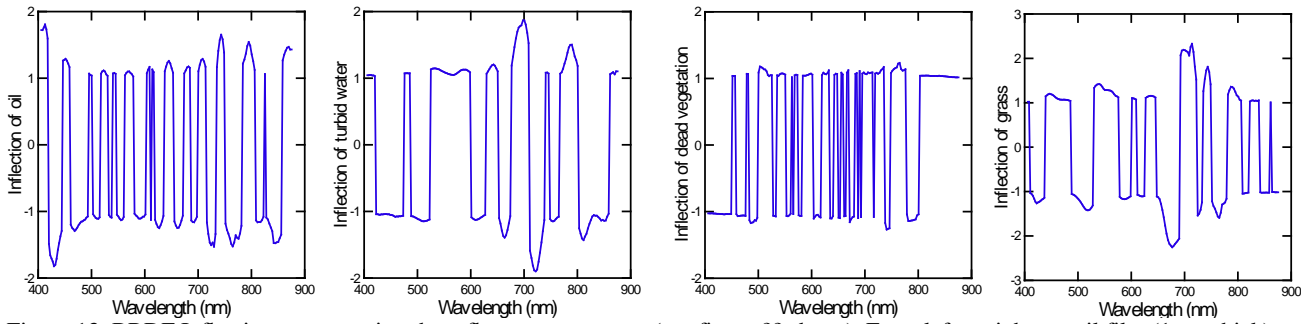


Figure 13. BRDF Inflection spectra using the reflectance spectrum (see figure ?? above). From left to right: an oil film (1mm thick) on clear water, turbid water, dead vegetation (dead leaves) and grass.

The inflection algorithm can also be applied to the contrast spectra (to enhance variation in the contrast spectrum). The result of this calculation is given in the following figures.

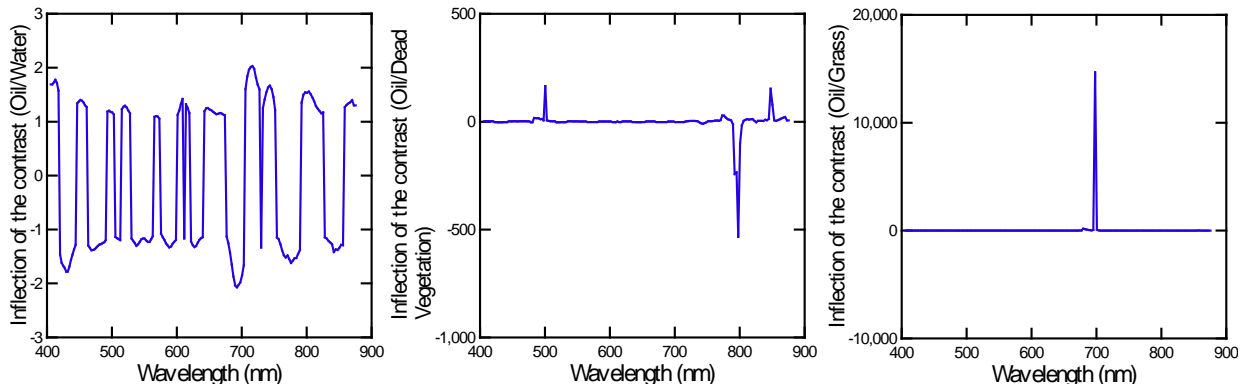


Figure 14. Inflection of the contrast spectra. The contrast target is weathered oil with different backgrounds. From left to right: turbid water, dead vegetation (dead leaves) and grass are the contrast backgrounds.

Once the inflection spectra are calculated, it is also possible to apply Weber's definition of the contrast to the inflection spectra instead of the BRDF. The resulting spectra are given in the following figure:

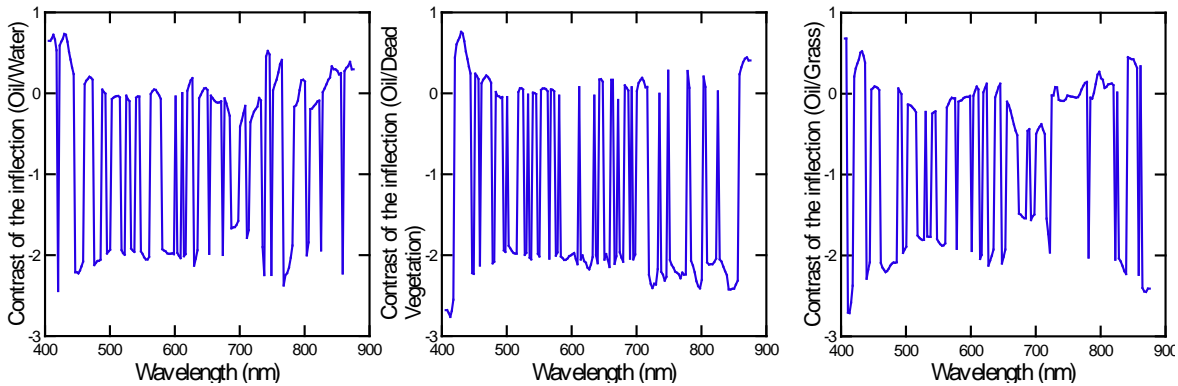


Figure 15. Weber contrast of the inflection spectra. The target is the oil with different backgrounds. From left to right: turbid water, dead vegetation (dead leaves) and grass. Optimal bands and spectral regions are indicated by the greatest positive or negative values across the spectrums.

The result of the optimization will yield a band or band ratio for the different types of contrast (Weber's contrast, contrast of the inflection or inflection of the contrast). The optimal bands using the different techniques that were obtained using the oil film as target and water, dead vegetation or grass as target are shown in the Table 1 and are used in processing hyperspectral imagery collected using the methods in the results section of this paper.

	Water	Dead vegetation	Grass
Weber's contrast	$Band(\lambda = 875nm)$	$Band(\lambda = 406nm)$	$Band(\lambda = 406nm)$
Inflection of the contrast	$Band(\lambda = 692nm)$	$Band(\lambda = 798nm)$	$Band(\lambda = 698nm)$
Contrast of the inflection	$Band(\lambda = 430nm)$	$Band(\lambda = 430nm)$	$Band(\lambda = 406nm)$
Multiple wavelength contrast	$\frac{Band(\lambda = 850nm)}{Band(\lambda = 405nm)} - 1$	$\frac{Band(\lambda = 875nm)}{Band(\lambda = 555nm)} - 1$	$\frac{Band(\lambda = 839nm)}{Band(\lambda = 555nm)} - 1$
Multiple wavelength contrast of the inflection	$\frac{Band(\lambda = 722nm)}{Band(\lambda = 413nm)} - 1$	$\frac{Band(\lambda = 741nm)}{Band(\lambda = 413nm)} - 1$	$\frac{Band(\lambda = 714nm)}{Band(\lambda = 430nm)} - 1$

Table 1. Resulting bands or band ratios for the optimization of: the contrast (Weber's definition), the inflection of the contrast, the contrast of the inflection spectra, the multiple wavelength contrast (as defined above) and the multiple wavelength contrast of the inflection spectra. In each situation oil is the target and the background is: water (turbid water), dead vegetation or field grass.

2.5 Collection of Hyperspectral Imagery from Littoral Zone Shore Data

In order to detect and discriminate the presence of weathered oil on a near shore habitat or the spatial extent of weathered oiled along a shoreline, a novel and new technique has been developed for collecting HSI imagery from a small vessel (anchored or underway), or the sensor mounted in the littoral zone. The resulting HSI imagery produces pixel sizes or ground sampling distances (GSD) on the order of several mm to cm scales, depending upon the distance between the sensor and the shoreline. The purpose of collecting this type of imagery is to (1) reduce atmospheric affects and (2) minimize the influence of the "mixed pixel" and "adjacency effects" in selecting spectral regions for detection of weathered oil and for testing algorithms. The results are also immediately and directly applicable to low altitude airborne imagery, especially if the same sensor is used aboard the airborne platform.

The sensor used to view the shoreline can be directly mounted on the vessel or can be mounted above the water but near the shore using a tripod or in a vessel. In the case of a mounted sensor on a vessel, the vessel is anchored at two points, allowing movement in mainly one direction (for example the boat is anchored to mainly allow motion due to waves in the pitching direction. Fixed platform mounting does not require motion correction, however the data collected from the anchored vessel requires roll motion correction (in this case pitch correction). In order to perform this correction, an IMU (inertial measurement unit) is attached to the HSI sensor and collects the sensor motion information while the pushbroom sensor sweeps or is rotated (using a rotation stage) along the shoreline being investigated. This correction will be applied before any further processing of the contrast algorithms are applied to the imagery taken in the Northern Gulf of Mexico and shown below. An example of the measurement scheme that has been used to detect and discriminate weathered oil is shown below.

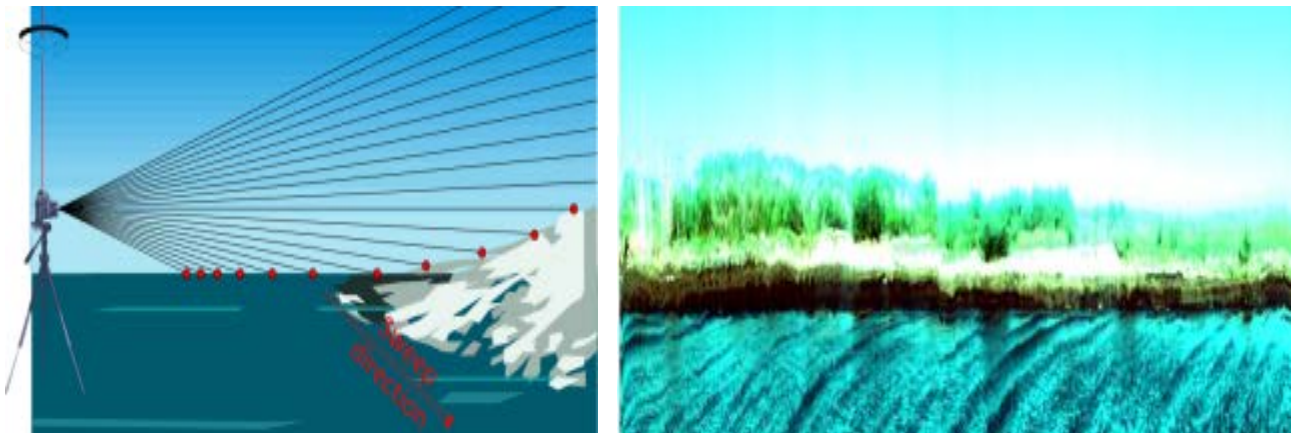


Figure 16. Left: the HSI imaging system is placed upon a small vessel or a fixed platform (tripod) in shallow water types within viewing distance of a shoreline. The sensor sweeps the shoreline and the pushbroom sensor produces a hyperspectral image of the shoreline as shown in the above HSI 3 band image. Note the ability to see gravity and capillary waves, small grasses on the shoreline as well as weathered oil at the land-water margin. Image collected February 28, 2011 in Barataria Bay, Louisiana

The image above is the resulting hyperspectral image 3 band RGB display of a shoreline that has been impacted by a recent oil-spill in the Gulf of Mexico region, near Bay Jimmy, Louisiana. In this case a vessel mounted sensor was used and the image was corrected for the platform motion (right). To illustrate the influence of the motion of a small vessel, and the necessary IMU corrections needed, a shoreline was imaged from the vessel (below left image) and from a fixed *in-situ* platform (right image) in April 2011

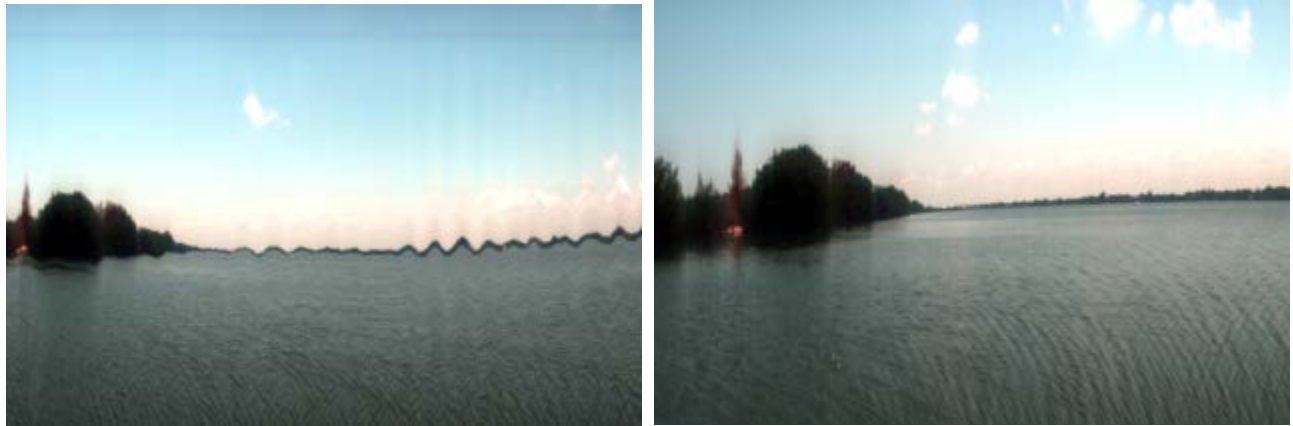


Figure 17. A hyperspectral image (left) 3 band RGB display of a littoral zone using a pushbroom sensor mounted on a vessel anchored at two points. During the acquisition of the hyperspectral image the sensor records the pitching effect of the anchored vessel that needs to be corrected using an IMU sensor due to the water surface gravity waves. The influence of this motion can clearly be seen in the image if no correction is applied (left). The shoreline area (right) acquired when the pushbroom sensor was mounted on fixed platform above the water. In this case no correction needs to be applied to the image. Note the clarity of the water surface capillary and small gravity waves.

3. RESULTS

3.1 Hyperspectral Scanline Geometric Corrections for Platform Motion Control

Images are presented below that shows the results of application of the Kalman filtering approach in order to correct for moving platform directional changes using a GPS and IMU sensor roll corrections.



Figure 18. An acquired airborne image from the HSI spectral cube (bands: 487, 529, 683nm) collected 3/20/2011. The above image shows the uncorrected image (the blue line is due to a calibration correction and shows the continuously acquired scan lines). The imagery was taken at an altitude of 1225m. The pixel size (GSD) is approximately 50 cm² with a swath width of approximately 0.8 km. The image was collected approximately 4 PM local time during a sequence of flights in the Pensacola, Florida area.

The image below (top) shows the results of applying a Kalman filter using only 5 HZ GPS data to correct for the moving platform directional changes. Note the curvature in the side of the image indicates directional change and the shift in the scan lines applied as a result of using the GPS position information. The images have not yet been georeferenced. The bottom image shows the image after GPS and IMU roll sensor data are used to correct the hyperspectral image cube.

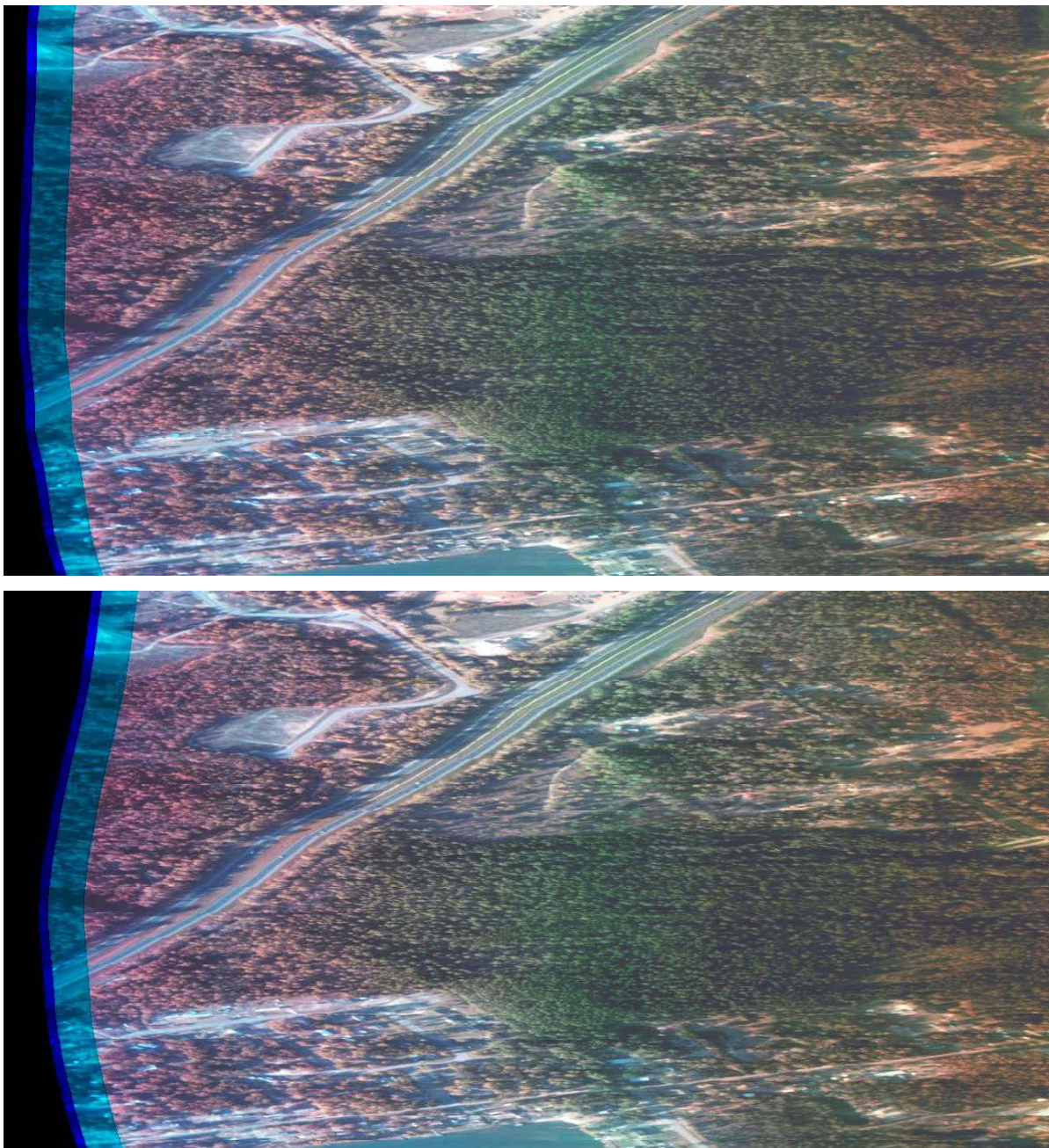


Figure 19. Airborne image from the HSI spectral cube (bands: 487, 529, 683nm) collected 3/20/2011. The top image shows resulting image corrected for GPS directional changes only. The lower image shows the image after being corrected for directional change and the IMU roll motion derived sensor information. The HSI image was acquired at an altitude of 1225m. The pixel size (GSD) is approximately 50 cm^2 with a swath width of approximately 0.8 km. The image was collected approximately 4 PM local time during a sequence of flights in the Pensacola, Florida area where oil spill impacts were previously found in coastal littoral areas.

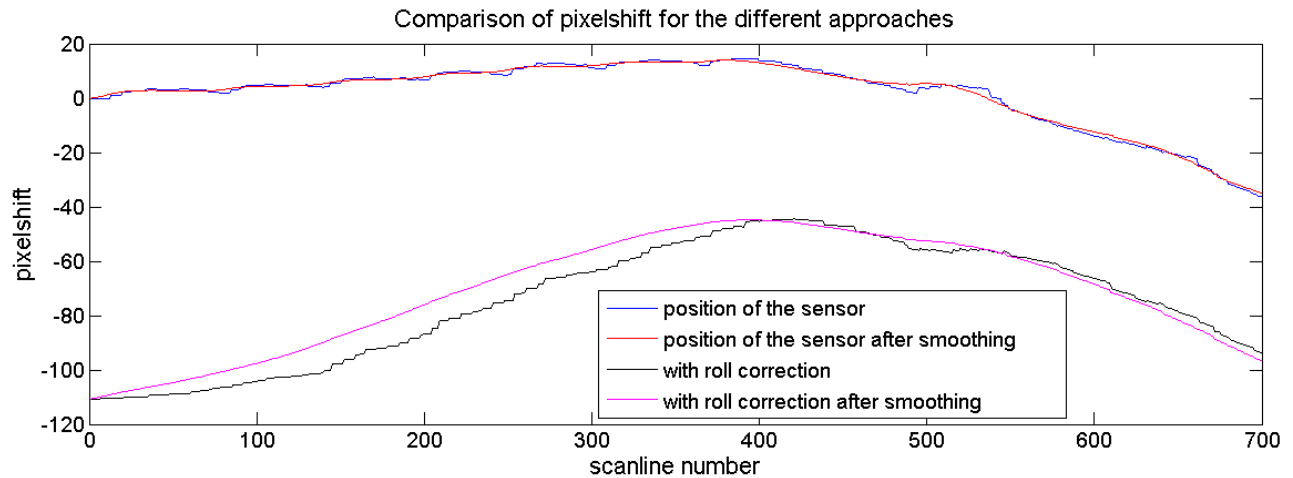


Figure 20. Comparison between the calculated “pixelshift” values in the cross-track direction for the different Kalman approaches described in the text. The top blue and red curves show the shift due to the change in position of the sensor respectively before and after smoothing using 5 HZ WAAS differential corrected GPS sensor data. The lower black and pink curves show the shift correspondent to the change in position of center scanline pixel on the ground corrected for the influence of the GPS and roll motion respectively before and after smoothing.

3.2 Optimal Band Selection Algorithms Applied to Oil detection in a Hyperspectral Imagery in Littoral Areas in the Northern Gulf of Mexico

In the section 2.5 optimal bands were found to detect a target (weathered oil film) with respect to a several different backgrounds. This procedure was applied on reflectance spectra collected with a spectrometer. But this same procedure can be applied to airborne or littoral zone imagery collected from a vessel or a fixed platform us HSI. Using knowledge of the water spectra, vegetation or dead vegetation spectra, the optimal contrast algorithm results can be applied to the image spectra. In image results shown below, images were processed using the data presented in Table 1.



Figure 21. Result of the band selection on a hyperspectral image where oil is the target to be discriminated and water is the background. On the left is a composite RGB image of the optimal bands found using the reflectance spectra with the red channel of 875nm – optimal value for Weber’s contrast, the green channel at 692nm – optimal value for the inflection of the contrast spectrum, and blue channel of 430nm – optimal value for the contrast of the inflection spectra shown in Table 1. On the right is a composite RGB image of the optimal bands found the HIS derived red channel of 811nm – optimal value for the contrast of the inflection spectra, green channel of 758nm – optimal value of Weber’s kontras and the blue channel of 649nm – optimal value for the inflection of the contrast spectrum based upon HIS signatures analyzed from the hyperspectral signatures with oil as the target feature.

The following image gives the result of the optimal band ratios obtained using the reflectance spectra or using the HSI image where oil is the target and turbid water as background using a multiple wavelength contrast ratio.

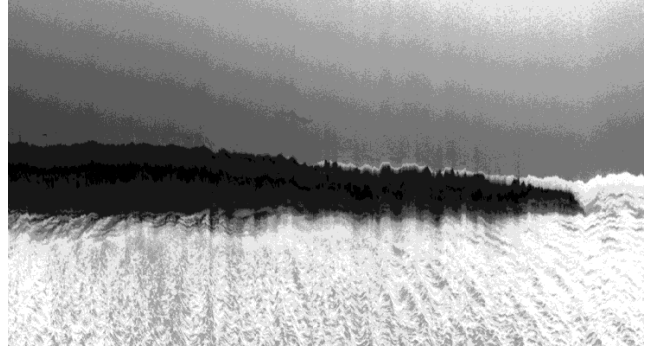
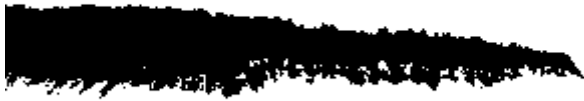


Figure 22. Result of the band selection on a hyper spectral image where weathered oil is considered the target and turbid water is the background. On the left is a grayscale image of the optimal band ratio (multiple wavelength of the inflection) using the reflectance spectra ($Band(\lambda = 722nm) / Band(\lambda = 413nm) - 1$). On the right is a gray scale image of the optimal band ratio (multiple wavelength of the inflection) using the HIS optimal band ratio ($Band(\lambda = 514nm) / Band(\lambda = 755nm) - 1$).

3.3 Simultaneous Hyperspectral & Large Format Photogrammetric Imagery of the Land and Water Surface for Detecting Weathered Oil Spill and Remediation Activity Impacts

In Figure 1, a scanned multispectral image (left) and a simultaneously obtained hyperspectral image (right) that both clearly suggested plumes of weathered oil in nearby littoral waters. The HSI image was extracted from a corrected airborne flight track shown below. The circled area shows the area identified using the HSI image. Upon zooming into the 255 Megapixel multispectral image it was found that remediation of the wetland and island littoral zone was underway - due to the presence of oil containment booms, vessels and people observable in the image as shown below. This was observed at several locations and the oil plumes were evident at several locations in the littoral areas as shown below.

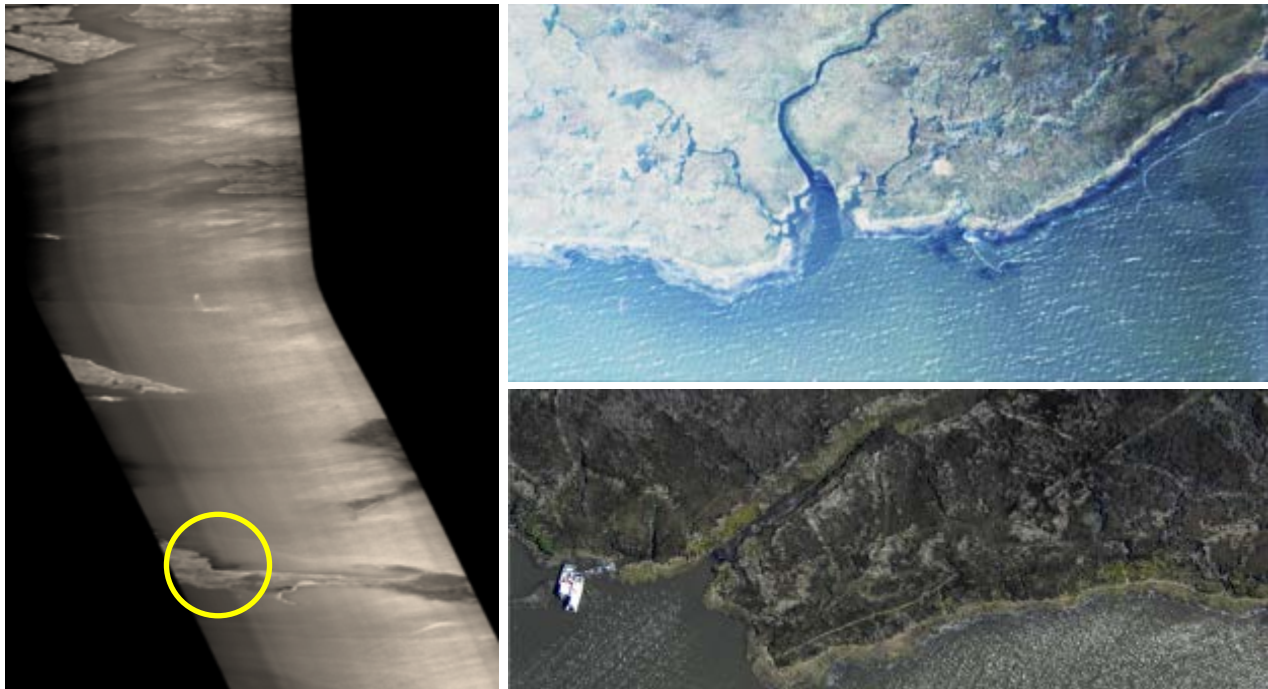


Figure 23. A hyperspectral airborne flight track corrected for flight direction (left). The zoomed areas are areas show remediation activities and weathered oil being released into the nearby littoral zone waters. Vessels and booms are visible suggesting disaster remediation and weathered oil containment activities. Imagery collected March 21, 2011 at 4,500 ft. altitude using 3 different simultaneous imaging systems aboard the moving platform.

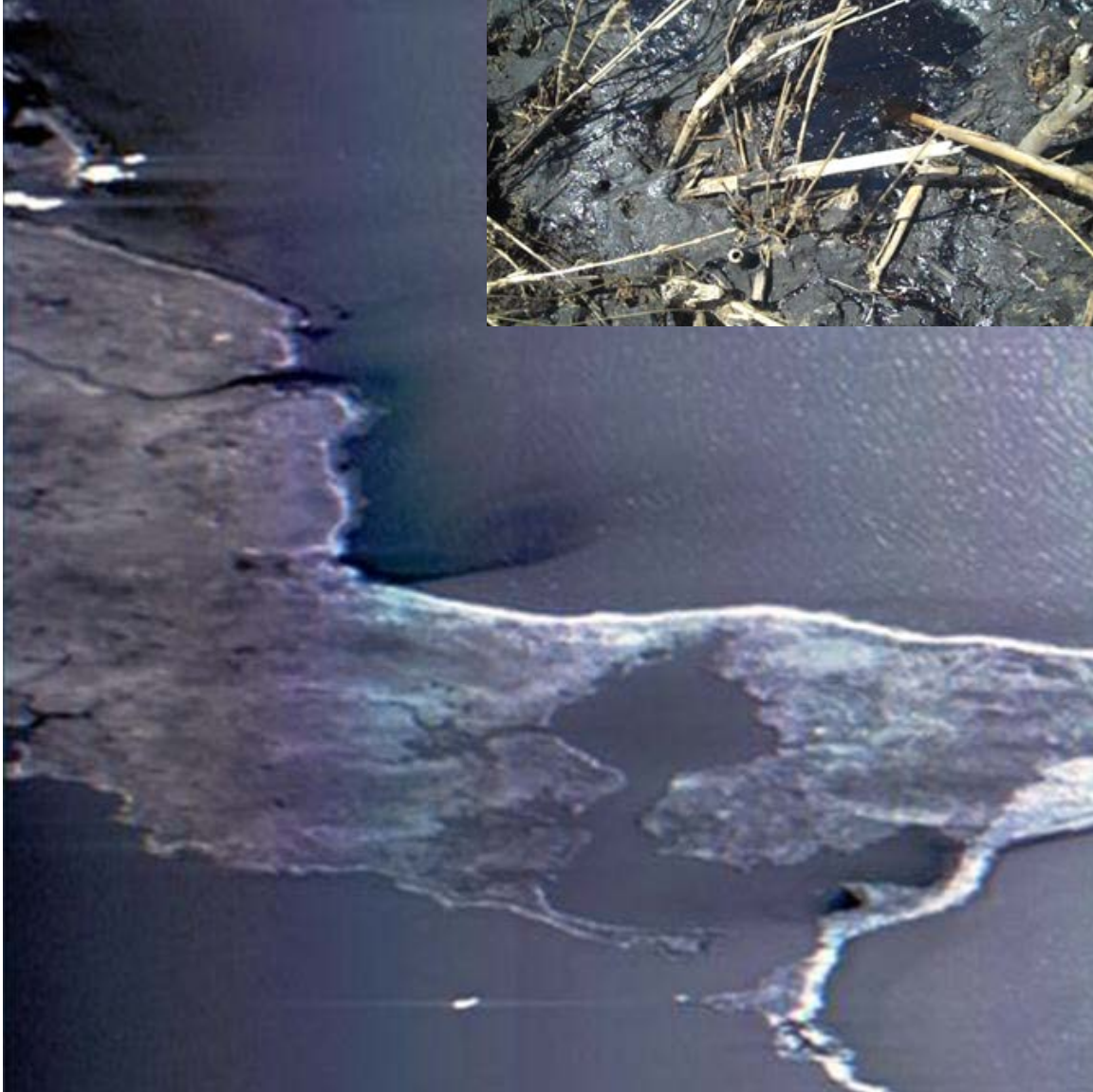


Figure 24. A HSI 3 band image subset that has been corrected for platform motion (bands: 540, 532, 525 nm) obtained March 21, 2011 in Jimmy Bay Louisiana. The hyperspectral image with 0.7 meter pixel size shows the plumes of weathered oil in the littoral zone waters. A close-up view of weathered oil in this area is shown in the upper corner.

4. SUMMARY AND CONCLUSIONS

The purpose of this paper has been to describe different calibration approaches and techniques useful in the development and application of remote sensing imaging systems and data for environmental monitoring, surveillance-maintenance from mobile platforms. Calibration includes the use of laboratory and field techniques including the scanning of photogrammetric negatives utilized in large format cameras, as well as *in-situ* targets and spectral wavelength and radiance calibration techniques. A newly integrated hyperspectral airborne pushbroom imaging system has been described in detail. Imagery from different integrated imaging systems were described for airborne remote sensing algorithm development using high spatial resolution (on the order of a few cm^2 to larger sub meter pixel sizes) imaging systems. The high spatial and spectral resolution hyperspectral imagery requires correction for platform motions and this has been accomplished using Kalman smoothing and filtering algorithms. Optimal bands or spectral channels have been selected and a technique demonstrated for image enhancement of selected channels from the corrected hyperspectral

imagery. Research is underway to use the multi-platform imagery and suite of sensors for spectral-spatial sharpening and data fusion techniques. The Gulf of Mexico oil spill disaster is an excellent example of the need for mobile platform and sensors to help provide needed environmental monitoring and surveillance-maintenance interventions of robotic and moving platforms to collect data for immediate as well as future decision-making purposes

5. ACNOWLWDGEMENTS

The work presented in this paper has been supported in part by the Northrop Grumman Corporation, NASA, Kennedy Space Center, KB Science, the National Science Foundation, the US-Canadian Fulbright Program, and the US Department of Education, *FIPSE* & European Union's grant *Atlantis STARS* (Sensing Technology and Robotics Systems) to Florida Institute of Technology, the Budapest University of Engineering and Economics (BME) and the Belgium Royal Military Academy, Brussels, in order to support of the involvement of undergraduate students in obtaining international dual US-EU undergraduate engineering degrees. Acknowledgement is also given to recent funding from a *Florida Institute of Oceanography's BP Corporation's* research grant award in support of aerial image acquisitions.

6. REFERENCES

- [1] Bostater, C., "Imaging Derivative Spectroscopy for Vegetation Dysfunction Assessments", SPIE Vol. 3499, pp. 277-285 (1998)
- [2] Bostater, C., Ghir, T., Bassetti, L., Hall, C., Reyier, R., Lowers, K., Holloway-Adkins, K., Virnstein, R., "Hyperspectral Remote Sensing Protocol for Submerged Aquatic Vegetation in Shallow Water", SPIE Vol. 5233, pp. 199-215 (2003)
- [3] Aktaruzzaman, A., Simulation and Correction of Spectral Smile Effect and its Influence on Hyperspectral Mapping, MS Thesis, International Institute for Geo-Information Science and Earth Observation, Enschede, Netherlands, pp. 77 (2008)
- [4] Bostater, C., Jones, J., Frystacky, H., Kovacs, M., Joza, O., "Image Analysis for Water & Subsurface Feature Detection In Shallow Waters", SPIE Vol. 7825, pp. 7825-17-1 to 7, (2010).
- [5] Roy, D. P., Devereux, B., Grainger, B., White, S.J., "Parametric geometric correction of airborne thematic mapper imagery", Int. J. Remote Sensing, 18 (9), p.1865-1887 (1997)
- [6] Welch, G., Bishop, G., [An Introduction to the Kalman Filter]. Course notes, Department of Computer Science, University of North Carolina, Chapel Hill, North Carolina (2006)
- [7] Sarkka, S., Vehtari, A., Lampinen, J., "CATS benchmark time series prediction by Kalman smoother with cross-validated noise density", Neurocomputing (Amsterdam) (0925-2312), 70 (13-15), p. 2331 (2007)
- [8] Nicodemus, F.E., 1970. Reflectance nomenclature and directional reflectance and emissivity, Appl. Optics, 30, 4427-4438pp
- [9] Apel, J.R., 1987, Principles of Ocean Physics, International Geophysics Series – Volume 38, Academic Press 589p.
- [10] Peli, E., 1990, Contrast in complex images, Journal of the Optical Society of America, A/Vol. 7, No. 10/October 1990, 2032p
- [11] Bostater, C., Hall, C., and Breininger, D., 1992, High resolution optical signatures and band selection techniques for endangered species and habitat management, International Symposium on Spectral Sensing Research, Volume I, 15-20 November 1992, Maui, Hawaii, USA.
- [12] Bostater C., 1992, Remote sensing research using aircraft and ships for estimating optimum band and coefficients related to ecosystem responses, In: Proceedings First International Conference on Remote Sensing of Marine and Coastal Environments, New Orleans 12p.